Supporting Information

A Universal Mobile Electrochemical Detector Designed for Use in Resource-Limited Applications

Alex Nemiroski[a], Dionysios C. Christodouleas[a], Jonathan W. Hennek[a], Ashok A. Kumar[b], E. Jane Maxwell[a], Maria Teresa Fernández-Abedul[c], and George M. Whitesides[a,d,e]

[a] Department of Chemistry & Chemical Biology, Harvard University, Cambridge, MA 02138
[b] School of Engineering and Applied Science, Harvard University, Cambridge, MA 02138
[c] Departamento de Química Física y Analítica, Universidad de Oviedo, Asturias, Spain
[d] Wyss Institute for Biologically Inspired Engineering, Harvard University, Cambridge, MA 02138 USA
[e] The Kavli Insitute for Bionano Science, Harvard University, Cambridge, MA 02138 USA

Corresponding author: George M. Whitesides (gwhitesides@gmwgroup.harvard.edu)

SUPPORTING DATA

Current and future usage of mobile phones in the developing world. We compiled data on current and projected mobile phone usage for Brazil (1, 2), Russia (3-5), India (6, 7), China (8), Indonesia (9)**,** SSA (10) and present the data in Figure S1.

EXPERIMENTAL DESIGN

Device Design and fabrication. We used the microcontroller to sample and compute data acquired from the potentiostat, to encode and decode frequency-modulated data, and to display a graphical user interface (GUI) on the LCD. We configured six digital input/output channels to operate the external DAC, ADC, and LCD over a serial peripheral interface (SPI) protocol, and one digital output channel to transmit data over audio by frequency shift keying (FSK). We configured four analog input channels to sample the voltages associated with the potentiostat, one analog input channel to receive data over audio, and three digital input channels to detect the states of the buttons.

Device Fabrication. We mounted these electronics on a custom-made printed circuit board (Advanced Circuits) and housed all components in a plastic case that we fabricated by 3D-printing (Fortus 250mc, Stratasys). The assembled device measured 56 mm x 106 mm x 18mm and weighed 63 g. The bill of materials (BOM) was ~$25 (not counting the case, and assuming a purchase volume of at least 1000 components each). We show the full circuit diagram in Figure S2 and the BOM in Table S1.

Design of the Potentiostat. Together with a feedback resistor R_f, the op-amp controlling the working electrode formed a transimpedance amplifier (TIA), converting the current I into an output voltage $V_o = V_w - IR_f$ while maintaining the working electrode at V_w, set by the DAC. The feedback resistance R_f set the sensitivity of the system. We chose R_f = 8 kΩ for all measurements, and suitable DC offsets for all electrodes in order to place the desired measurements in the range of the potentiostat.

To set V_R and V_W V_R and V_W, we chose a two-channel, 16-bit DAC (DAC8552, Texas Instruments) programmed by the popular 3-wire SPI protocol. The smallest potential step required in our applications was ~5 mV, and since the nonlinearity of most DACs is within a few least-significant bits (LSB), the 16-bit resolution provided us with sufficient voltage resolution (3.3 V / 2^{16} ~ 0.05 mV) to ensure that any non-idealities in the voltage generation were at most a few percent of the smallest voltage steps. We updated the output of the DAC at a rate ~2 kHz although, in principle, the system could support rates up to ~20 kHz if necessary. To sample the output signal with high resolution, we also incorporated a 16-bit ADC. With its required 1.25-V reference, this ADC provided us with a resolution of 1.25 V / 2^{16} ~ 20 μV, although the practical minimum voltage that we could resolve was limited by the voltage noise of ~ 40 μV_{rms}, as measured by the ADC, which for R_f = 8 kΩ , corresponded to a current resolution of ~ 5 $nA_{rms.}$ For most measurements, however, we averaged the signal over 5 seconds (100 consecutive data points) to reduce the electronic noise to ~0.5 nA_{rms}. We found, in all cases, that the electrochemical noise was substantially (10–100x) greater

than the electronic noise. Therefore, for all pulse sequences, we also configured the uMED to apply a 30-point smoothing function on all traces automatically to reduce the electrochemical noise. After the uMED performed these various forms of signal averaging automatically, it then extracted a concentration by comparing to a saved calibration or sent the acquired values to a PC for further analysis.

Acquisition of Data. To evaluate the performance of the device, however, we needed to extract the raw data from the device. We interfaced with and collected raw data from the uMED by connecting a personal computer to the serial port of the uMED through a serial-to-USB converter (FT232RL, FTDI). We developed a custom application in MATLAB (Mathworks, Natick MA) to acquire, convert, and display raw data received over USB from the uMED. Once we calibrated the uMED for chronoamperometry, SWASV, and potentiometry, we programmed the microcontroller to perform these measurements (e.g. signal averaging, baseline correction, peak extraction) automatically, without an external computer.

Modes of Electrochemical Detection. Figure S3 shows a scheme of the time and voltage sequences implemented for the different types of measurements and, where necessary, the expected transient behavior of the measured current.

For **CV**, the uMED sweeps the potential E applied between the RE and WE linearly from E_1 to E_2 (and back again), and measures the current I consumed by the electrochemical cell. Steps in voltage E_{step}, each held for a duration t_{step}, form a staircase ramp with a scan-rate E_{step},/ t_{step},. CV is the most widely used technique for acquiring information about electrochemical properties (e.g. redox potentials) of the species in the reaction mixture and of the electrode surface (11, 12) or, in some cases, to assay analytes (13).

For chronoamperometry, the uMED applies a potential step E between the counter electrode (CE) and WE for a fixed duration and measures the transient current I. Typically, the current I will be dominated by i) an initially large, non-Faradaic, capacitive decay that is related to total area (including surface roughness) of the electrodes and not to the concentration C of the analyte; then by ii) a slow Faradaic, Cotrellian decay that is proportional to the concentration ($I \propto Ct^{-1/2}$); and finally iii) a Faradaic steady-state current proportional to the concentration ($I_0 \propto C$) and primarily due to radial diffusion around an electrode of finite size and convective disturbance of the diffusion layer (14). To suppress background currents and noise, the uMED i) begins sampling the current several seconds after the application of the voltage step (when the Faradaic current is dominant) and ii) averages I over a fixed length of time Δt to decrease the influence of random electrochemical and thermal fluctuations by a factor of $\sqrt{\Delta t}$.

For **DPV** and **SWV**, the uMED measures the current generated in the electrochemical cell during a series of regular voltage pulses (applied between the RE and WE) that are superimposed on a linear sweep from E_1 to E_2 have a peak-to-peak height ΔE, and a frequency $f = (t_1 + t_2)^{-1}$, where t_1 is the pulse duration and t_2 is the time between pulses. In these differential techniques, the device records the currents I_1 and I_2 immediately before a change in the applied voltage (i.e. at end of the

pulse); the peak value of the consecutive differences $\Delta I = I_1 + I_2$ is proportional to the concentration of the analyte ($\Delta I \propto C$) .

For **potentiometry**, the uMED measures the constant voltage E generated by the electrochemical species. To prevent destabilization of E, the uMED incorporates operational amplifiers with a high input impedance (~10^{12} Ω) that limit the current flowing during measurement to < 0.1 pA.

Figure S3b shows an example of chronoamperometry in context of glucometry. Figure S3c shows an example of these DPV and SWV used in context of anodic stripping voltammetry (ASV). In DPV, the differential current is formed by consecutive values $\Delta I(n) = I_2(n) - I_1(n)$, where $I_1(n)$ is the current immediately before forward pulse n, and $I_2(n)$ is the current at the end of forward pulse n. For this type of measurement, $t_2 \gg t_1$ to allow the solution to attain a diffusive equilibrium before each forward voltage pulse. In SWV, the differential current is formed by consecutive values $\Delta I(n) = I_2(n) - I_1(n + 1)$, where $I_1(n + 1)$ is the current at the end of reverse pulse $n + 1$(immediately before the next forward pulse). For this type of measurement $t_2 = t_1$ to suppresses the contribution of background Faradaic processes to the signal, to enable a faster voltage sweep than DPV.

Procedure for Performing a POC Test. Table S2 lists the general procedure for some of the tests that can be performed with minimal training (after initial calibration) and for uploading data over voice.

Network Connection, Packet Structure, and Error Correction. Figure S4 shows a flow of data from a POC measurement to a remote facility. We employed a simple packet structure with two sections: i) a header to identify the type of measurement being transmitted (glucose, lead, sodium, or malaria) and ii) a body to store the numeric data, modified by the CRC. The header contained a single 50-ms tone that identified whether the data being transmitted corresponded to glucose (f = 1600 Hz), lead (f = 1700 Hz), sodium (f = 1800 Hz), or malaria (f = 1900 Hz). The body contained an integer-valued, base-10 representation of the concentration of a single measured analyte, encoded with the CRC. We encoded each integer in the sequence by a 50-ms tone at a frequency corresponding to the integer value. Since the ATmega328 can only output digital signals, we represented data as a sequence of square wave tones and passed the output through a passive, low-pass filter to attenuate all but the lowest-order, sinusoidal harmonic. In our implementation, we used a 10-bit CRC (0b1000000001) that enables detection of errors for sent values up to $2^{10} = 1024$. For larger values, it would be necessary to use a longer CRC for to reliably detect errors.

Power Consumption. The total number of measurements N the uMED can perform on a single battery charge can be calculated by

$$N = \frac{Q_{BATT}}{\langle I \rangle \cdot T}, \tag{1}$$

Where Q_{BATT} is the battery lifetime, $\langle I \rangle$ is the average current consumption, and T is the total time spent in operation. The rechargeable, 3.7-V lithium-polymer battery (PL-651628-2C, AA Portable Power Corp) that we used had a lifetime Q_{BATT} = 210 mAH. The uMED consumed

$\langle I_{stby} \rangle$ = 10 mA during standby (no measurement). The current consumption during measurements ranged from $\langle I_{gluc} \rangle$ = 11 mA for glucometry (T_{gluc} = 20 s) to $\langle I_{ASV} \rangle$ = 24 mA for ASV (T_{ASV} = 280 s), for which the power consumption was dominated by the vibration motor used for mixing. For an initially fully charged battery, these values indicate that the uMED can perform a maximum of N_{gluc} ~ 3440 glucose measurements or N_{ASV} ~ 110 ASV measurements before depletion. Depending on which measurements are performed and the frequency of use, the uMED can, therefore, last from one to several months before needing to be recharged.

MATERIALS AND METHODS

Chemical Reagents. All chemicals were used without further purification. For evaluating the performance of the different electrochemical pulse sequences we used potassium ferrocyanide, potassium ferricyanide, 1-napthol, sodium chloride, and potassium chloride purchased from Sigma-Aldrich. For detection of heavy metals we used sodium chloride (NaCl, 99.999%), sodium acetate Trace SELECTA (99.999%), water trace SELECT Ultra (AGS reagent), bismuth standard for AAS (999 ± 4 mg/L), cadmium standard for ICP (1000 ± 2 mg/L), zinc standard for ICP (1000 ± 2 mg/L), and lead standard solution for ICP/OCP (10.127 ppm) purchased from Sigma-Aldrich. For detection of recombinant *Pf*HRP2 (PIP001 from AbD Serotec) we used 96-well plates (Costar 3590) from Corning, anti-*Plasmodium falciparum* antibody (ab9206) and anti-*Plasmodium falciparum* horseradish peroxidase conjugate detection antibody (ab30384) from Abcam, bovine serum albumin (BSA), and Tween-20 from Sigma-Aldrich, and Ultra TMB-ELISA from ThermoScientific. For the determination of glucose in assayed blood samples and the determination of sodium in assayed urine samples we used the Liquicheck Urine Chemistry Control Levels 1 and 2 (LOT 64360) and Trilevel minipole control Meter Trax Control (LOT 92510) from BioRad.

Materials and Instrumentation. For evaluation of chronoamperometry, cyclic voltammetry, SWV, and DPV we used unmodified screen-printed carbon electrodes (DRP110) from DropSens. For potentiometry we used ion-selective electrodes for sodium (K27504-30) and potassium (WU-27504-26) purchased from Cole-Palmer. For detection of glucose we used commercial test strips (TRUEtrack, Nipro Diagnostics). For SWASV and chronoamperometric detection of *Pf*HRP2 we used carbon nanotube-modified SPEs (DRP110-CNT) from DropSens, for enhanced sensitivity.

Measurement Procedure. For measurement of glucose we used a new test strip for each measurement. For detection of heavy metals, we measured the entire dilution series (6 samples, including the blank) on a single SPE in order of increasing concentration. We performed seven replicates of this series of measurements, each with a new SPE. We conditioned each new SPE by first performing a full sequence on a sample with no metal ions to ensure the electrode was free of any contaminants that could be removed by sampling conditions. After the cleaning step of each measurement, we rinsed the electrode with ultrapure DI water and dried with N_2. For detection of

malaria, we measured the entire dilution series (5 samples, including the blank) on a single SPE in order of increasing concentration. We performed seven replicates of this series of measurements, each with a new SPE. Before taking measurements with a new electrode, we performed chronoamperometry at E = 0.2 V for 40 s on a solution of PBS to ensure the electrode was free of any contaminants that could be removed by sampling conditions. Each SPE was rinsed with PBS and dried with N_2 between each measurement.

Glucometry. The glucose test strips that we use have a pair of electrodes (WE and CE) defined by carbon ink, and all of the necessary reagents (e.g., enzymes and electrochemical mediator) pre-stored on the test strip. A typical hand-held glucometer uses a two-electrode (counter and working) potentiostat to apply a simple voltage sequence that consists of an incubation period at zero applied voltage, followed by a measurement period at a fixed applied voltage (typically E = 0.5 V). The glucose oxidase (an enzyme) present in the test strip converts glucose (the analyte) and potassium ferricyanide (an electrochemical mediator) to gluconic acid and potassium ferrocyanide, the oxidation of which can be measured by chronoamperometry, which is one of most common techniques for monitoring an enzymatic reaction that produces a redox-active species, such that the measured current correlates to the concentration of the redox species. We adapted this type of sequence and programmed the uMED to first apply E = 0.5 V to test for the presence of the sample in the reaction zone (Figure S3B). With the test strip inserted, but no sample present, there were no mobile ions to carry charge (current) between the electrodes. When we placed a sample on the test strip, the presence of ions in the solution gave sufficient conductivity to the test zone that it could be measured as current. In principle, this technique can also be adapted to analytes other than glucose that are amenable to chronoamperometric detection at 0.5 V. We and others have demonstrated that glucometers using this type of pulse sequence can also quantify lactate, cholesterol and ethanol (15), cocaine, adenosine, and uranium (16) or a specific DNA aptamer (17).

Detection of Heavy Metals by SWASV. To test the device for detection of metals (Zn(II), Cd(II) and Pb(II)) in water samples we first prepared a solution containing all the necessary reagents: 2 mg/L of bismuth ions as a co-deposition agent in a solution of 0.5-M acetic acid, 0.5-M sodium acetate, and 0.25-M sodium chloride. Next we prepared a series of sample solutions of Zn, Cd, and Pb ions (blank and 2–40 µg/L each) in water. To measure the concentration of these ions, we mixed 20 µL of the reagent solution with 80 µL of the sample solution on the top of the SPE and activated the uMED to perform the SWASV sequence automatically.

Malaria Immunoassay with Chronoamperometric Detection. Preparation of the 96-well plates was performed following the procedure by Noedl *et al.* (18). We coated high-binding 96-well plates with 100 µl of a 1.0-µg/mL solution of anti-*Plasmodium falciparum* antibody in PBS (1x). The plates were sealed and incubated overnight at 4°C after which the supernatant was discarded and the wells were incubated with 200 µL/well of 2% bovine serum album (BSA) in PBS for 2 hrs. After washing three times in 0.05% Tween-20 PBS, the plates were sealed and

stored at -20 °C until use. Recombinant *Pf*HRP-2 was diluted in PBS to the desired concentration (0–200 ng/ml) and 100 µL was added to each well followed by 1 h incubation at RT. The wells were washed three times with PBS-Tween solution before the addition of 100-µL anti-*Plasmodium falciparum* horseradish peroxidase conjugate detection antibody at a concentration of 0.5 µg/ml in a solution of PBS with 2% BSA and 1% Tween-20. After 1 h incubation at RT, wells were washed in PBS-Tween solution three times. The final washing solution was left in the well until just before the addition of 100 µL of Ultra TMB-ELISA. The TMB solution incubated at RT for 2 min. in the dark before the reaction was stopped with 50 µL of 10% sulfuric acid (v/v). A 75-µL drop was immediately placed on the SPE. Chronoamperometry was performed at E = 0.2 V for 20 s. The potential used for amperometry was selected by first performing at CV scan from E_1 = 0 V to E_2 = 0.7 V at a scan-rate of 0.03 V/s step size of E_{step} = 2.5 mV. The position of the oxidation and reduction peaks is highly dependent of the pH of the system. We chose E = 0.2 V to ensure that reduction can be completed with minimal contribution from oxidation.

We programmed the uMED to automatically check whether the output current followed the expected chronoamperometric sequence (monotonically increasing and reaching a stable plateau after ~ 20 s) by automatically discarding any sequences for which $I(t - 5s) - I(t) < -0.043$ V (a value that we determined empirically) for any time t. This process is similar to the way a hand-held glucometer displays an error message when the chronoamperometric sequence yields data that is not consistent with the expected transient behavior.

Verification of Packet Structure and Data Throughput. It is important that physiological, medical, and environmental data received by a remote computer be correct. Our choice of CRC error detection guarantees that any three-digit value can be determined to be completely error free after transmission. This reliability, however, does not prevent corrupt data from arriving at the destination, effectively slowing down the transmission rate to the time it takes to deliver a correct packet of data. The rate at which packets are corrupted depends on the quality of the data channel and the method of decoding used. Figure S5A–C shows a frequency-modulated packet with a randomly chosen value, its frequency spectrum, and its decoded value. We sent the data from the uMED, through a Nokia 1112, over the AT&T voice network, and received it with through a custom MATLAB application via Skype on a remote personal computer. We sampled the data at 44.1 kHz, and performed a rolling Fast Fourier Transform to analyze the frequency content of the packet and decode the sequence of integers. We characterized the effect of errors during transmission on the average throughput of data by determining the packet success rate (*PSR*) by

$$\mathrm{PSR} = \frac{\#\ \text{uncorrupted packets}}{\#\ \text{sent packets}}, \tag{1}$$

and the effective packet rate (EPR) by $EPR = PSR \cdot PR$, where PR is the raw packet rate (packets / s). The *EPR* quantifies the average rate at which correct packets are received, and signifies the average throughput of uncorrupted data.

Figure S5D–F shows how the PSR and EPR depend on the symbol rate—the rate at which individual digits are transmitted. We characterized the PSR and its effect on the EPR by i)

establishing a live connection to a remote computer through a mobile phone, ii) sending a sequence of packets containing random numeric data, encoded by CRC, from the uMED to the remote computer, and iii) comparing the received packets with the sent packets to determine the fraction of corrupted packets. We found that the PSR was constant around 98% at low symbol rates, but increased dramatically above 25 symbols/s, where the symbols begin to be too short to be properly identified with a simple FFT due to the distortion present in the voice channel. We found that the EPR is maximized at 29 symbols/s, indicating an optimal tradeoff between PER and the PR. Each packet consisted of average of six digits of CRC-encoded, numeric data (20 bits)— including three digits of underlying numeric data (10 bits)—and header (2 bits). At the maximal EPR (1.4 packets/s), the effective bitrate of CRC-encoded data and header was 31 bits per second (bps) and the effective bitrate of the underlying data and header was 17 bps.

Although we used a binary header, there was enough bandwidth to signify up to 16 different identifiers (4 bits), which would increase the effective bit rates by 3 bps each. We never identified an instance where the CRC failed to properly discriminate between corrupted and uncorrupted packets of data. When receiving data from a user, the remote computer responds with an ACK as soon as it receives a single uncorrupted packet. The signal delay between the user and the remote computer can vary depending on signal strength and other factors, but is usually approximately 0.5 seconds. We found that at the optimal EPR, the median time a user had to wait for an ACK after beginning to send data was 2.2 seconds.

Biochemical Stability Defines the Temperature Range of the System. For some tests, the chemistry or biochemistry (e.g. enzymatic kinetics, stability of proteins and reagents, rates of electrochemical reactions), and some physical properties of the system (e.g. viscosity of liquids, and rates of mass transport) may be the source of temperature dependent properties. In fact, any system relying on molecular recognition or enzymatic processes will have the same issues with (possibly) limited ranges of temperature. This device accomplishes the readout of chemical processes using electronic components that are stable with temperature, and therefore the operating temperature range of the system will be determined largely or entirely by its chemistry and biochemistry.

Low cost and battery operation enable affordable replacement. By making the device small and inexpensive, we address a critical problem in the developing world: repair or replacement when a device is damaged (e.g., by a power surge, or by misuse). It is, in practice, very difficult or impossible to arrange repair in many parts of the developing world because parts and repair technicians are not available, and this difficulty compromises the usefulness of larger (and perhaps more automated) devices intended for central laboratory use. Our device is designed to deal with this issue in two ways. First, by making it as inexpensive as possible, it can simply be replaced when it is broken. For example, a $50 device (which is more expensive than we would anticipate in large-scale production) that is used for 1000 tests before it was damaged (a number much lower than we would anticipate for this device) would contribute only $0.05 per test to the

cost of the delivered test. Second, by making the device very efficient in use of power, it is possible to operate it from batteries; battery operation automatically protects it against certain common problems in wall power (especially surges) in the developing world. It is, thus, designed more on the power model of the cellphone rather than a developed-world clinical analyzer.

STOCK IMAGES

We used stock images of smartphones and electrodes in Figure 1B of the main text. Here we include links to the original images.

3G Smartphone (Blackberry Curve) from
http://cmvlive.com/wp-content/uploads/2011/10/Blackberry-Curve-9360-300x264.jpg

4G Smartphone (Apple iPhone 5s) from
http://images.apple.com/iphone-5s/specs/images/dimensions_2x.jpg

Ion-Selective Electrode (Cole Palmer) from
http://static.coleparmer.com/large_images/2750212.jpg

Glucose Test Strip (True Trak) from
http://img.medicalexpo.com/images_me/photo-g/blood-glucose-test-strips-94055-6140961.jpg

Screen-Printed Electrode (DropSens) from
http://www.mep.net.au/wpmep/wp-content/uploads/2013/01/DropSens_201203_DRP_BI10_sf_w980X360.jpg

SUPPORTING REFERENCES

1. eMarketer, Inc. (2013) Mobile Rivals PCs for Brazil's Internet Audience. Available at: http://www.emarketer.com/Article/Mobile-Rivals-PCs-Brazilrsquos-Internet-Audience/1010311 [Accessed March 9, 2014].
2. eMarketer, Inc. (2014) 2013: The Year of the Smartphone in Latin America. Available at: http://www.emarketer.com/Article/2013-Year-of-Smartphone-Latin-America/1010545 [Accessed March 9, 2014].
3. eMarketer, Inc. (2013) Russia's Digital Ecosystem Shaped by Market Nuances. Available at: http://www.emarketer.com/Article/Russias-Digital-Ecosystem-Shaped-by-Market-Nuances/1009653 [Accessed March 9, 2014].
4. eMarketer, Inc. (2014) Forecast: mobile phone users in Russia 2011-2017. Available at: http://www.statista.com/statistics/274770/forecast-of-mobile-phone-users-in-russia/ [Accessed March 9, 2014].

5. eMarketer, Inc. (2013) Major Bump in Mobile Web Use in Urban Russia. Available at: http://www.emarketer.com/Article/Major-Bump-Mobile-Web-Use-Urban-Russia/1010076 [Accessed March 9, 2014].

6. eMarketer, Inc. (2014) Forecast: Smartphone user penetration in India 2010-2016. Available at: http://www.statista.com/statistics/257048/smartphone-user-penetration-in-india/ [Accessed March 9, 2014].

7. eMarketer, Inc. (2014) Forecast: Mobile phone users in India 2011-2017. Available at: http://www.statista.com/statistics/274658/forecast-of-mobile-phone-users-in-india/ [Accessed March 9, 2014].

8. eMarketer, Inc. (2013) The Mobile Ad Boom Reaches China. Available at: http://www.emarketer.com/Article/Mobile-Ad-Boom-Reaches-China/1010293 [Accessed March 9, 2014].

9. Rao M (2012) Mobile Southeast Asia Report 2012: Crossroads of Innovation. *Mobile Monday*. Available at: http://www.mobilemonday.net/reports/SEA_Report_2012.pdf.

10. Analysys Mason (2013) Smartphone Take-Up in Sub-Saharan Africa Will Grow Rapidly, Although Pricing Concerns Will Limit Adoption. Available at: http://www.analysysmason.com/About-Us/News/Insight/Smartphone-take-up-SSA-Mar2013/ [Accessed March 9, 2014].

11. Huang K-J, Niu D-J, Xie W-Z, Wang W A disposable electrochemical immunosensor for carcinoembryonic antigen based on nano-Au/multi-walled carbon nanotubes–chitosans nanocomposite film modified glassy carbon electrode. *Anal Chim Acta* 659:102–108.

12. Etienne M, Guillemin Y, Grosso D, Walcarius A (2012) Electrochemical approaches for the fabrication and/or characterization of pure and hybrid templated mesoporous oxide thin films: a review. *Anal Bioanal Chem* 405:1497–1512.

13. Saurina J, Hernández-Cassou S, Saurina J, Fàbregas E, Alegret S (1999) Determination of tryptophan in feed samples by cyclic voltammetry and multivariate calibration methods. *Analyst* 124:733–737.

14. Bard AJ, Faulkner LR (2000) *Electrochemical Methods* (Wiley).

15. Nie ZZ, Deiss FF, Liu XX, Akbulut OO, Whitesides GMG (2010) Integration of paper-based microfluidic devices with commercial electrochemical readers. *Lab Chip* 10:3163–3169.

16. Xiang Y, Lu Y (2011) Using personal glucose meters and functional DNA sensors to quantify a variety of analytical targets. *Nature Chemistry* 3:697–703.

17. Xiang Y, Lu Y (2012) Using Commercially Available Personal Glucose Meters for Portable Quantification of DNA. *Anal Chem* 84:1975–1980.

18. Noedl H et al. (2005) Simple histidine-rich protein 2 double-site sandwich enzyme-linked immunosorbent assay for use in malaria drug sensitivity testing. *Antimicrob Agents Chemother* 49:3575–3577.

Figure S1: Comparison of relative usage of smartphones vs. non-smartphones (low-end phones) in Brazil, Russia, India, China, Indonesia, and Sub-Saharan Africa (SSA) in (**A**) 2014, (**B**) 2016-2017 (projected), and (**C**) combined.

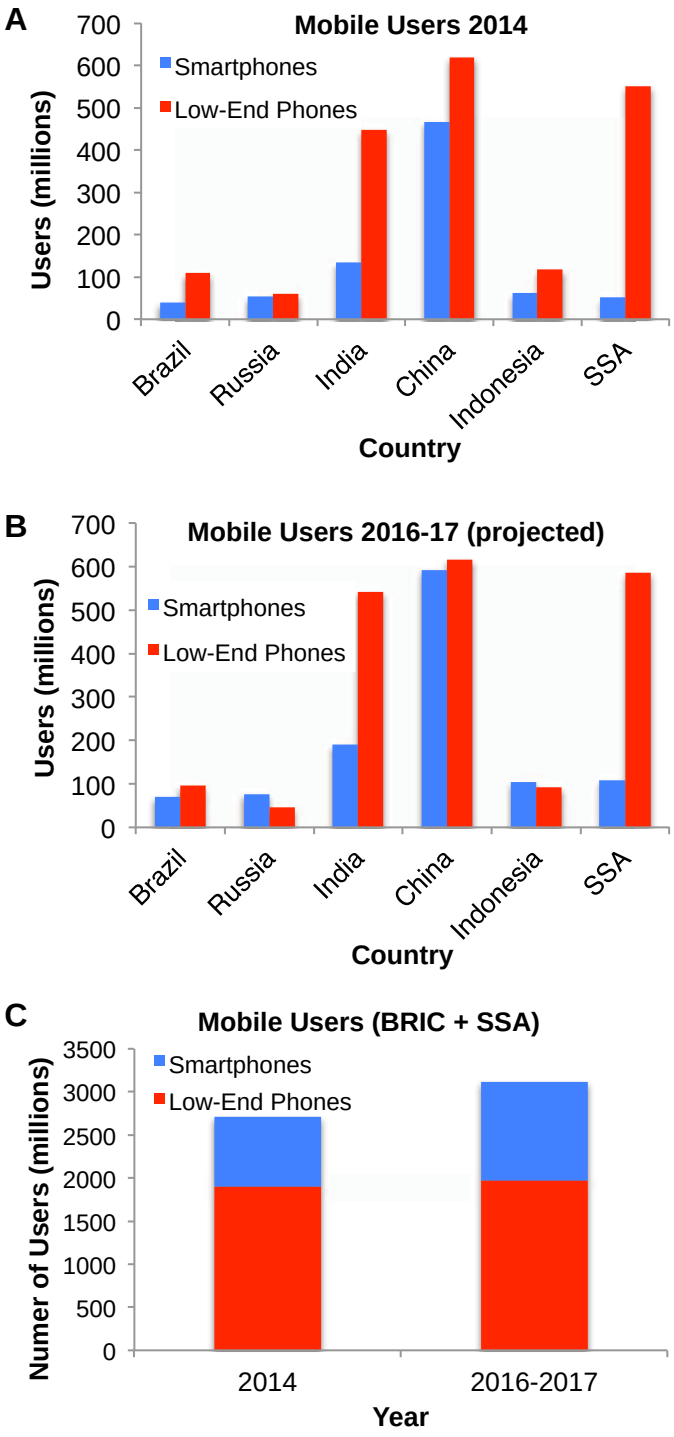

Figure S2: Full Circuit Diagram for uMED.

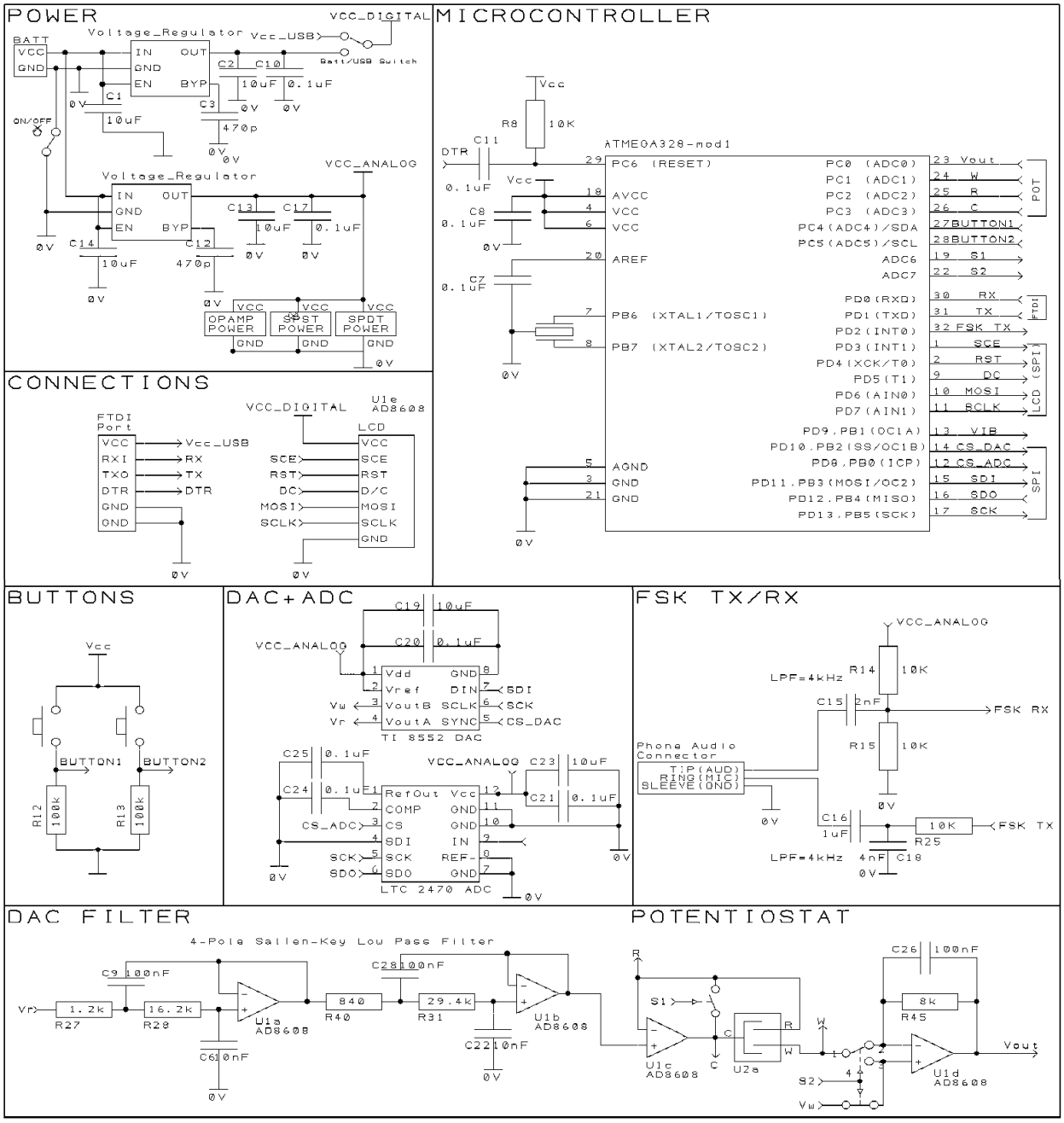

Table S1: Bill of Materials for the uMED. For the price, we quote for >1000 units.

Description	Part No	Quant.	Price Ea.	Total	Vendor
JST Right-Angle Connector	455-1719-ND	1	$0.07	$0.07	Digikey
Polymer Li-Ion Cell (3.7V, 210mAh)	PL-651628-2C	1	$2.65	$2.65	BatterySpace
IC LDO Regulator (3.3V, SOT23-5)	576-1259-1-ND	2	$0.39	$0.78	Digikey
Microcontroller (ATMEGA328P)	ATMEGA328P-AU-ND	1	$1.77	$1.77	Digikey
2.5 mm 4 Conn Audio Jack (SMD)	CP1-42534SJTR-ND	1	$0.39	$0.39	Digikey
AD8608 Quad R-R Opamp	AD8608ARUZ-ND	1	$1.96	$1.96	Digikey
DAC8552 16-bit DAC (Dual Channel)	296-20676-1-ND	1	$3.99	$3.99	Digikey
LTC2470 16-bit ADC (Single Channel)	52R9827	1	$2.37	$2.37	Newark
Graphic LCD 84x48 - Nokia 5110	SKU091069	1	$2.83	$2.83	Banggood
Resonator 8.00 MHz Ceramic (SMD)	490-1195-1-ND	1	$0.25	$0.25	Digikey
Resistor: 0603	*n/a*	11	$0.00	$0.02	Digikey
Capacitor: 0402 (<= 0.1 uF) Ceramic	*n/a*	18	$0.00	$0.03	Digikey
Capacitor 0402 (1uF) Ceramic	587-1231-1-ND	1	$0.01	$0.01	Digikey
Capacitor 0805 (10uF) Ceramic	587-1300-1-ND	4	$0.01	$0.06	Digikey
Capacitor 1206 (10uF) Tantalum	495-2174-1-ND	2	$0.04	$0.08	Digikey
Analog Switch SPST (Dual Channel)	MAX4643	1	$1.01	$1.01	Mouser
Analog Switch SPDT (Single Channel)	MAX4644	1	$0.86	$0.86	Mouser
Vibration Motor, Flat Coin	28821-ND	1	$3.99	$3.99	Digikey
PCB	*custom*	1	$1.03	$1.03	4PCB
			TOTAL	**$24.15**	

Figure S3: Examples of the timed sequence of applied potentials and measurement for a representative sample of possible pulse sequences. (**A**) Cyclic voltammetry. (**B**) Chronoamperometry in the context of glucometery. (**C**) SWV and DPV in the context of ASV. We use the shaded regions to indicate the times when the current is recorded.

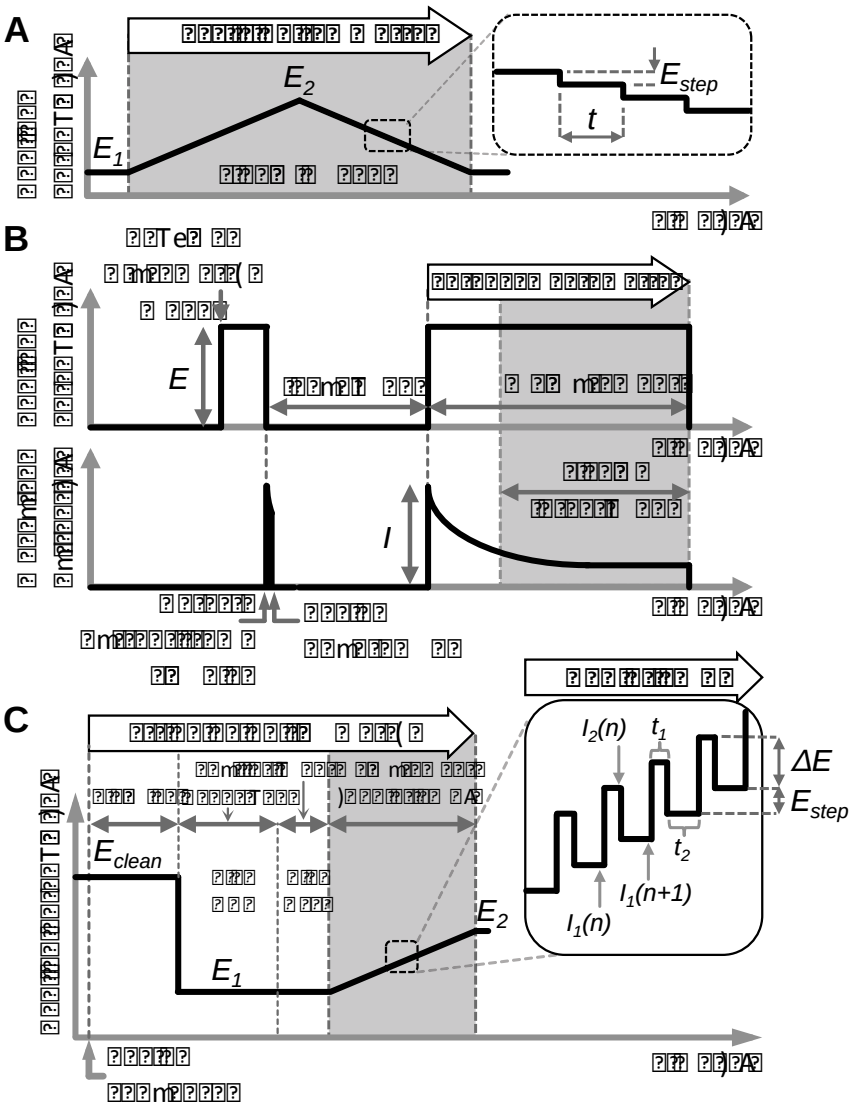

Table S2: Basic procedure for using the uMED for i) glucometry, ii) detection of lead in water, iii) detection of sodium in urine, and iv) uploading the results of testing over a mobile phone.

Glucometry:	**Lead Detection:**	**Sodium Detection**
1. Insert Glucose Test Strip 2. Select "Detect Glucose" from the uMED on-screen menu 3. Apply the sample: • Prick finger and wick into the test strip 4. After 15 seconds, the measured concentration automatically to appears on-screen	1. Insert SPE 2. Select "Detect Lead" from the uMED on-screen menu 3. Apply sample to electrode zone • 80 uL sample • 20 uL of reagent 4. Press button to begin test 5. After 5 minutes, the measured concentration automatically to appears on-screen	1. Attach ISE 2. Select "Detect Sodium" from the uMED on-screen menu 3. Collect sample into container 4. Add Buffer 5. Dip ISE into sample 6. Measured concentration automatically appears on-screen 7. Wait for value to stabilize
Uploading Data-over-Voice 1. Connect audio cable 2. Wait until data collection is finished 3. Call Medical Facility or Database 4. uMED automatically uploads data 5. Receive acknowledgment of data transfer on uMED 6. Receive text message (if applicable).		

Figure S4: A flow chart describing the sequence of operations involved in establishing error-free communication over a mobile voice network between the uMED and a remote computer. We developed a custom application in MATLAB to i) sample the audio stream received by VoIP, ii) analyze and identify the frequency content of each packet, iii) convert the sequence of tones into a corresponding sequence of integers, iv) identify the type of measurement, v) verify the integrity of the received data with a CRC, and if error-free, vi) log and display the data to the remote user, vi) play an acknowledgement (ACK) tone (5 s, 500 Hz) to the VoIP application, and vii) send the decoded value, or a diagnostic interpretation, to the local user's mobile phone in the form of a text message over short messaging service (SMS), sent through the web-portal of the chosen mobile carrier (here, AT&T). We configured the uMED to send packets continuously until it received an ACK from the remote computer and, upon receipt, to cease the transmission of data packets and display a message informing the user.

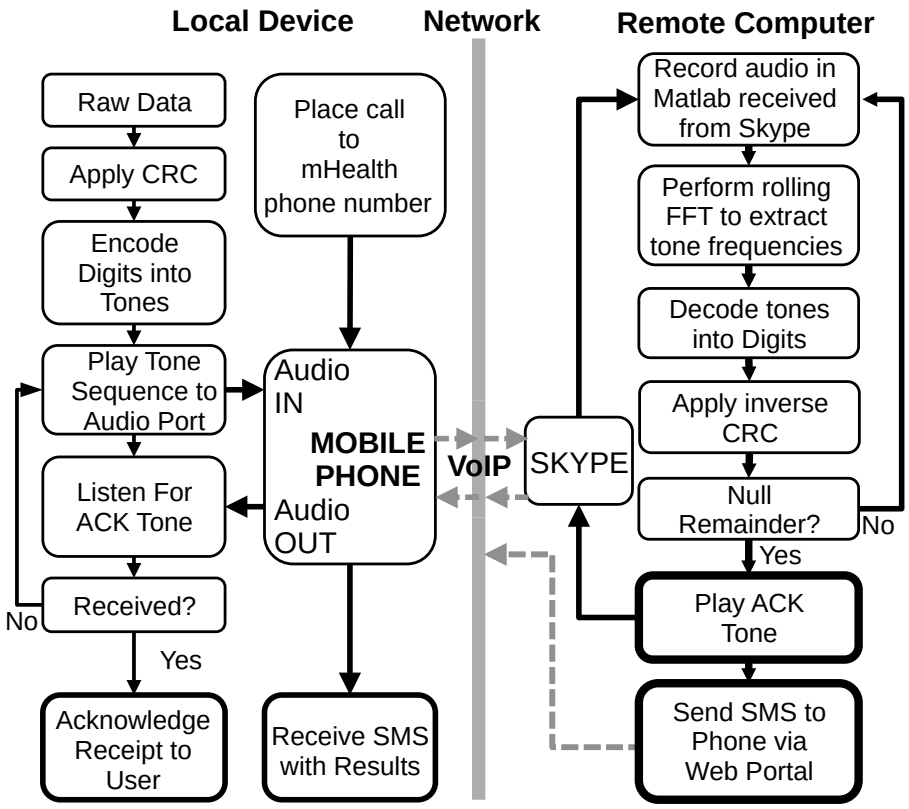

Figure S5: An example of a successfully transmitted packet and an analysis of the average throughput of data versus symbol rate. We encoded the randomly chosen value 274 mg/dL of glucose (encoded as 2-8-1-1-2-4-11 after CRC; the 11 corresponds to glucose) and transmitted it over an active voice connection. (**A**) The audio signal received by the DAQ application. (**B**) An FFT of the entire packet demonstrating the presence of seven distinct frequency signals and the values to which they correspond. (**C**) The decoded packet containing the sequence (read in reverse) 2-8-1-1-2-4-11, which, after removing the CRC value, decodes to the value 274-11, or 274 mg/dL of glucose. (**D**) The overall PSR versus the symbol rate. (**E**) The PR versus the symbol rate. (**F**) The EPR versus the symbol rate ($\mathrm{EPR} = \mathrm{PSR} \cdot \mathrm{PR}$). The optimal EPR = 1.4 packets/s occurred at 29 symbols/s. The error bars in (D) signify the standard error of the mean $\varepsilon_{\mathrm{PSR}} = \sqrt{\frac{\mathrm{PSR}(1-\mathrm{PSR})}{\mathrm{N}}}$, where p is the packet success rate, and $\mathrm{N} = 300$. The error bars in (B) are propagated from (A) by $\varepsilon_{\mathrm{EPR}} = \sqrt{\left(\frac{\partial \mathrm{EPR}}{\partial \mathrm{PSR}}\varepsilon_{\mathrm{PSR}}\right)^2 + \left(\frac{\partial \mathrm{EPR}}{\partial \mathrm{PR}}\varepsilon_{\mathrm{PR}}\right)^2}$, where $\varepsilon_{\mathrm{PR}}$ is the measured standard deviation in PR.